Distinct Characteristics of Inferonasal Fundus Autofluorescence Patterns in Stargardt Disease and Retinitis Pigmentosa

Tobias Duncker,[1] Winston Lee,[1] Stephen H. Tsang,[1,2] Jonathan P. Greenberg,[1] Jana Zernant,[1] Rando Allikmets,[1,2] and Janet R. Sparrow[1,2]

[1]Department of Ophthalmology, Columbia University, New York, New York
[2]Department of Pathology and Cell Biology, Columbia University, New York, New York

Correspondence: Janet R. Sparrow, Department of Ophthalmology, Columbia University, New York, NY 10032; jrs88@columbia.edu.

Submitted: July 23, 2013
Accepted: September 17, 2013

Citation: Duncker T, Lee W, Tsang SH, et al. Distinct characteristics of inferonasal fundus autofluorescence patterns in Stargardt disease and retinitis pigmentosa. *Invest Ophthalmol Vis Sci*. 2013;54:6820–6826. DOI:10.1167/iovs.13-12895

Purpose. To report distinct characteristics of fundus autofluorescence (AF) patterns inferior to the optic disc in recessive Stargardt disease (STGD1) and retinitis pigmentosa (RP).

Methods. Short-wavelength (SW) and near-infrared (NIR) AF images were acquired from patients with STGD1 and RP. In SW- and NIR-AF images of STGD1 patients, gray levels (GL) on both sides of the demarcation line were measured.

Results. In STGD1, a demarcation line, which has been assigned to the closed optic fissure, was visible on SW-AF and NIR-AF inferior to the optic disc. In healthy subjects, this demarcation line is only visible by SW-AF. At 20° inferior to the disc center, AF levels on the nasal side were 25% (±11%) lower than on the temporal side in SW-AF images and 18% (±11%) lower in NIR-AF images. For both STGD1 and RP, the inferonasal quadrant exhibited distinct SW- and NIR-AF patterns compared with other fundus areas. Disease-related AF changes, such as flecks, appeared to respect the demarcation line as a boundary.

Conclusions. Disease-related AF patterns originating in RPE in STGD1 and RP appear to respect the demarcation line in the inferonasal quadrant of the fundus as a border. The visibility of the inferonasal demarcation line by NIR-AF in STGD1 but not in healthy eyes may indicate that increased levels of RPE lipofuscin modulate the melanin-related NIR-AF signal. This feature of NIR-AF images may aid in the diagnosis of STGD1 patients.

Keywords: ABCA4, fundus autofluorescence, lipofuscin, melanin, optic fissure, retinal pigment epithelium, retinitis pigmentosa, scanning laser ophthalmoscope, recessive Stargardt disease

The short-wavelength autofluorescence (SW-AF; 488 nm excitation) signal recorded at the fundus by confocal laser scanning ophthalmoscopy is primarily generated from lipofuscin in the RPE.[1] Abnormalities of the SW-AF distribution in retinal disorders are a valuable diagnostic tool and allow monitoring of disease progression. In recessive Stargardt disease (STGD1), increased levels of lipofuscin accumulate in RPE cells[2] owing to defective ABCA4 protein activity in photoreceptor outer segment disc membranes.[3–6] Consequently, SW-AF intensity is increased.[7] It is not well understood why the macula is more susceptible to the damaging effects of *ABCA4* mutations than the retinal periphery. Also unclear are the factors that influence disease progression towards the periphery.[8]

We recently reported that SW-AF images of healthy subjects often exhibit a curved, near-vertical demarcation line inferior to the optic disc. The line derives from an abrupt discontinuity in SW-AF intensity, with lower SW-AF levels on the nasal side. In describing this fundus feature, we proposed that the demarcation line indicates the location of the embryonic optic fissure that closes during ocular development.[9] Despite increased use of wide-field AF imaging and a growing interest in peripheral SW-AF findings,[10–12] previous clinical studies have not brought attention to this feature. Here, we have examined the implications of this demarcation line in terms of the clinical presentation of retinal disease. We demonstrated that the demarcation line inferior to the optic disc appears to be a boundary that some disease-related SW-AF patterns respect. Moreover, we found that since the demarcation line was visible by near-infrared autofluorescence (NIR-AF, 787 nm excitation) in STGD1 patients but not in healthy retinae,[9] this feature may be a useful diagnostic aid. In addition, the visibility of the demarcation line in NIR-AF images of STGD1 patients may further our understanding of the subcellular source of NIR-AF.

Methods

Short-wavelength autofluorescence images were acquired with a confocal scanning laser ophthalmoscope (cSLO) (Spectralis HRA+OCT; Heidelberg Engineering, Heidelberg, Germany) from patients with a clinical diagnosis of STGD1 or RP and from healthy subjects. The RP patients and STGD1 patients P7, P8, P9, and P10 were included in this study because their disease-related SW-AF patterns extended into the inferonasal region of the fundus. For all remaining STGD1 patients, additional NIR-AF images were obtained with another cSLO

TABLE. Summary of Demographic, Clinical, and Genetic Data

Patient	Condition	*ABCA4* Mutations	Sex	Age, y	Eye	Iris Color	Race/Ethnicity	BCVA Snellen (logMAR)
P1	STGD1	p.P1380L, p.G1961E	M	12	OS	Blue	White	20/100 (0.70)
P2	STGD1	p.P1380L, p.G1961E	F	17	OS	Brown	White	20/150 (0.88)
P3	STGD1	p.Q1003X, p.G1961E	M	25	OS	Brown	White	20/40 (0.30)
P4	STGD1	p.C54Y	F	48	OD	Blue	White	20/30 (0.20)
P5	STGD1	p.R2077W	F	52	OD	Blue	White	20/40 (0.30)
P6	STGD1	p.[L541P;A1038V]	M	13	OS	Brown	White	20/150 (0.88)
P7	STGD1	p.T972N, p.L2027F	F	14	OS	Blue	White	20/80 (0.60)
P8	STGD1	c.4537_4538insC, p.V1686M	M	49	OS	Brown	White	20/50 (0.40)
P9	STGD1	p.R1108H, p.P1380L	M	50	OS	Blue	White	20/200 (1.00)
P10	STGD1	c.5714+5G>A	F	34	OD	Blue	White	20/200 (1.00)
P11	STGD1	p.Q636H, p.G1961E	M	46	OD	Brown	Indian	20/400 (1.30)
P12	STGD1	c.5461-10T>C	M	35	OD	Brown	Black	20/400 (1.30)
P13	STGD1	p.R1640W	F	20	OD	Brown	Black	20/125 (0.80)
P14	STGD1	p.R290W	M	47	OS	Brown	White	20/40 (0.30)
P15	STGD1	p.A1773V, p.G1961E	M	18	OD	Brown	White	20/150 (0.88)
P16	AD RP	p.T17M*	F	23	OD	Brown	Hispanic	20/30 (0.20)
P17	AD RP	N/A	M	39	OS	Brown	White	20/20 (0.00)
P18	AR RP	N/A	M	50	OS	Green	White	20/20 (0.00)

AD, autosomal dominant; AR, autosomal recessive; BCVA, best corrected visual acuity; F, female; logMAR, logarithm of the minimum angle of resolution; M, male; N/A, not available.

* *RHO* mutation.

(HRA2; Heidelberg Engineering) using the indocyanine-green angiography mode without dye injection. The latter group of STGD1 patients having NIR-AF imaging were seen consecutively in the clinic. Pupils were dilated with topical 1% tropicamide and 2.5% phenylephrine, and photopigments were bleached for 20 seconds[13] before acquisition of SW-AF images. Using i2kRetina software (DualAlign LLC, Clifton Park, NY), we were able to generate fundus montages from overlapping individual images and to align images of the same field.

Nonnormalized 30° SW-AF images (without automatic histogram stretching for contrast enhancement) of the region inferior to the optic disc were acquired in a subgroup of 10 STGD1 patients (P1, P2, P3, P4, P7, P11, P12, P13, P14, and P15). Within the subgroup, nonnormalized 30° NIR-AF images of the same region were also obtained in five patients (P1, P2, P4, P14, and P15). Mean gray levels (GL, corrected for the zero light GL)[13] in these images were measured, nasal and temporal to the demarcation line at 20° inferior to the disc center with IGOR software (WaveMetrics, Lake Oswego, OR). For area sampling, two rectangles (100 × 25 pixels; separation, 50 pixels) were positioned on both sides of the demarcation line; this approach required rotation of the images in some cases. The nasal-to-temporal ratios of the mean GLs were calculated.

All procedures adhered to the tenets of the Declaration of Helsinki, and written informed consent was obtained from all subjects after a full explanation of the procedures was provided. The protocol was approved by the Institutional Review Board of Columbia University.

All STGD1 patients and one of the RP patients were referred for genetic screening for causal mutations. Mutations in the *ABCA4* gene were detected with the ABCR700 microarray and/or by next-generation sequencing. In all STGD1 patients, at least one definite mutation was found. Two mutations were found in 8 of 15 patients. Demographic and clinical patient information and genetic data are presented in the Table.

Statistical analyses were performed using Prism 5 (GraphPad Software, La Jolla, CA) and the statistical tests as indicated.

RESULTS

Healthy Subjects

The spatial distribution of SW-AF in the fundus of healthy subjects follows a characteristic pattern (Fig. 1). Centrally, the SW-AF signal is attenuated owing to absorption of the excitation light by macular pigment. Optic disc and blood vessels are also dark due to minimal or no SW-AF emission and blockage of the SW-AF signal, respectively. In the inferonasal quadrant, relatively lower nasal SW-AF levels are separated from higher SW-AF levels on the temporal side by a curved,

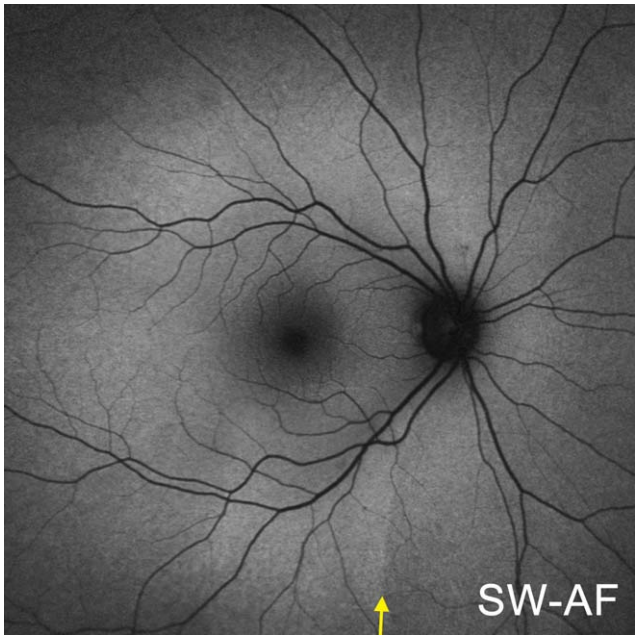

FIGURE 1. SW-AF fundus montage of a healthy subject. A near-vertical demarcation line, indicated by a *yellow arrow*, separates low SW-AF levels on the nasal side from higher SW-AF levels on the temporal side.

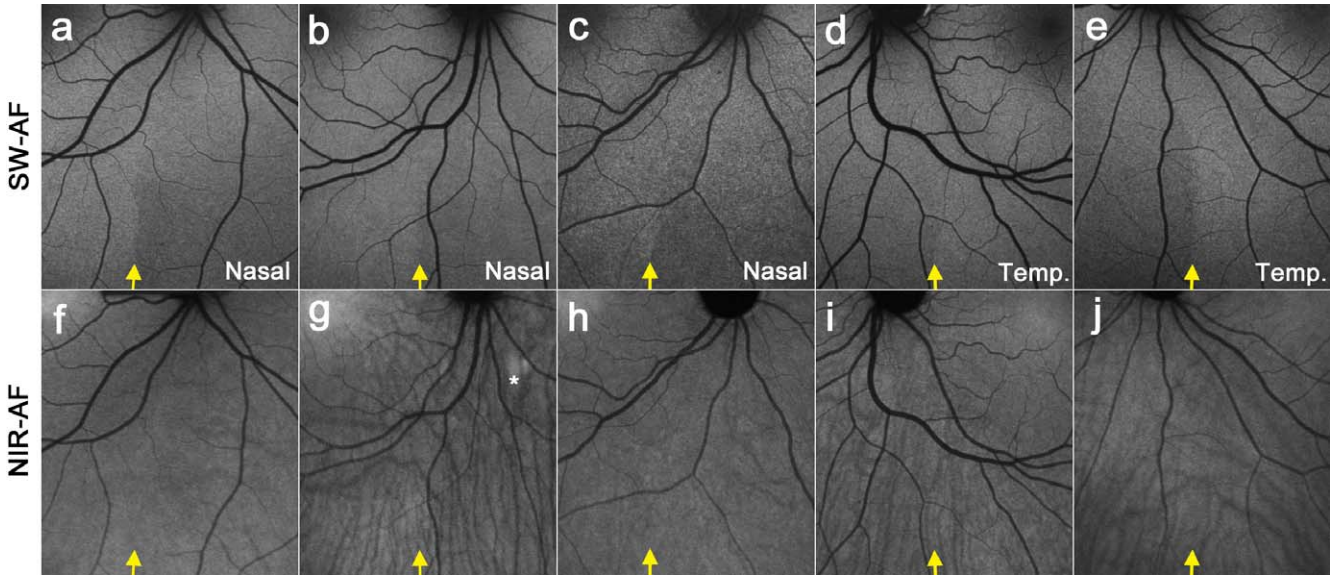

FIGURE 2. SW-AF and NIR-AF images of the fundus inferior to the optic disc obtained from healthy control subjects. SW-AF images are shown in the upper row (**a–e**), and NIR-AF images are in the lower row (**f–j**). A near-vertical demarcation line, indicated by a *yellow arrow*, separates low SW-AF levels on the nasal side from higher SW-AF levels on the temporal side. In the NIR-AF images (**f–j**), a demarcation line is not clearly visible at the corresponding position (*yellow arrow*), and the visibility of choroidal details is variable. (**g**) The choroidal nevus (*) exhibits increased NIR-AF signal.

near-vertical demarcation line (yellow arrow). This line likely represents the location of the closed optic fissure and was visible in 31 of 32 healthy subjects, although with varying degrees of contrast.[9] In the 17 healthy subjects used for comparison in this study, we did not observe an inferonasal demarcation line in NIR-AF images (Figs. 2f–j). The visibility of choroidal details in NIR-AF images can vary across subjects, which was also apparent in previous studies.[14–18]

Recessive Stargardt Disease

In STGD1, a demarcation line is visible at the same location on both SW-AF (Figs. 3a–e) and NIR-AF images (Figs. 3f–j). While not being clearly visible by NIR-AF in healthy subjects, the demarcation line was visible in all STGD1 patients that were examined in this study. Choroidal details are less visible in NIR-AF images of STGD1 patients (Figs. 3f–j) compared with healthy subjects (Figs. 2f–j).

While disease-related AF patterns in STGD1 may vary considerably depending on phenotypic differences and disease stage, the distribution of some phenotypic features may be modulated by the optic fissure. In P6 (Fig. 4), differences in orientation and density of flecks on one side of the demarcation line (yellow arrow) versus the other become apparent by both SW-AF (a) and NIR-AF (b). In Figure 5a, P7 exhibits a circular trail of flecks that are orientated around the

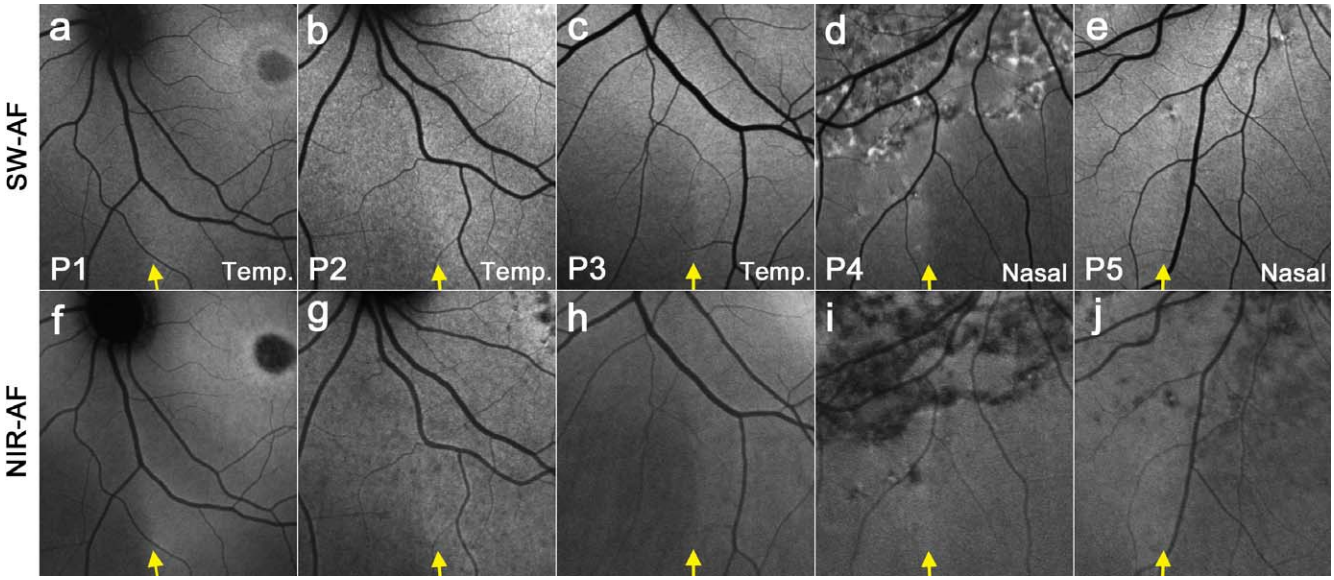

FIGURE 3. SW-AF and NIR-AF images of the fundus inferior to the optic disc obtained from STGD1 patients (P1, P2, P3, P4, and P5). SW-AF images are shown in the upper row (**a–e**), and NIR-AF images are in the lower row (**f–j**). Contrary to healthy subjects, a demarcation line is also visible by NIR-AF at the same position as in the SW-AF image (indicated by *yellow arrows*).

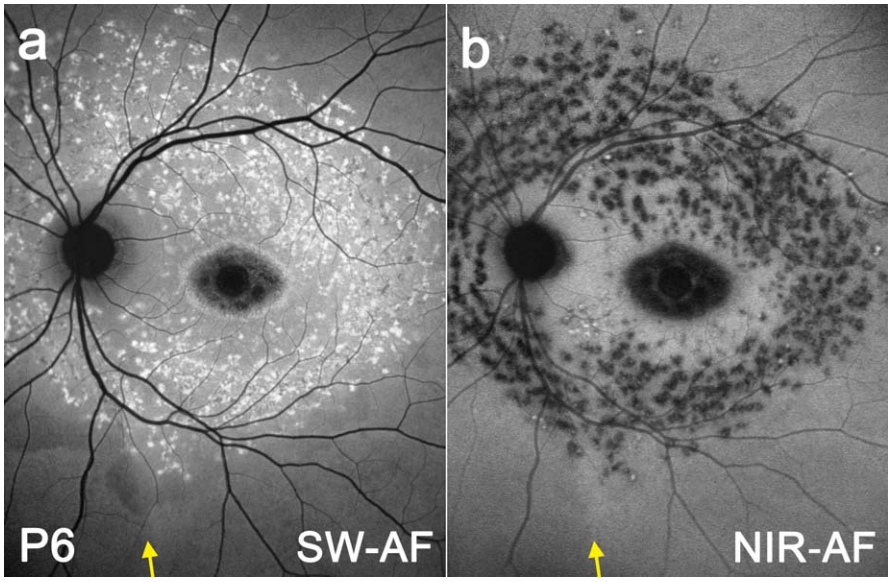

Figure 4. SW-AF (**a**) and NIR-AF (**b**) fundus montage of STGD1 patient P6. The optic fissure-related demarcation line is indicated by a *yellow arrow*.

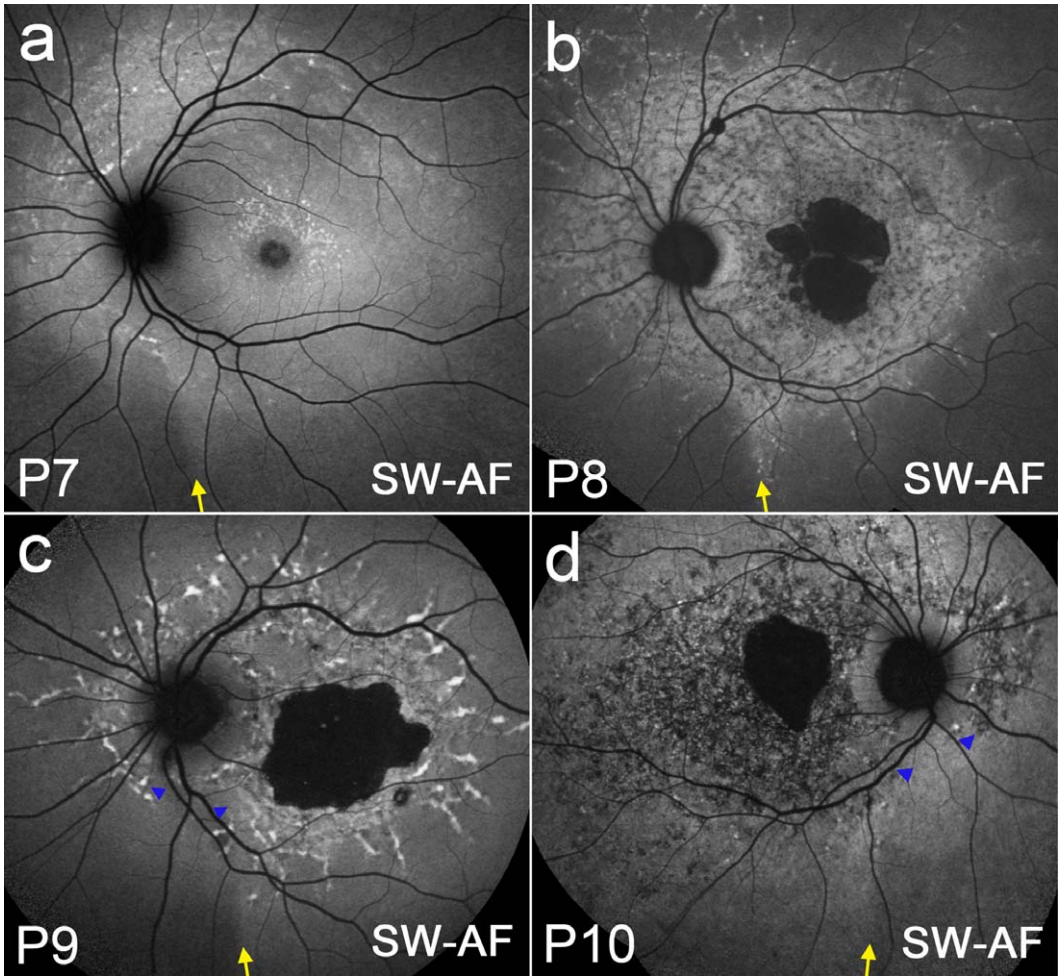

Figure 5. SW-AF fundus montages from STGD1 patients P7 (**a**), P8 (**b**), P9 (**c**), and P10 (**d**). The optic fissure-related demarcation line is indicated by a *yellow arrow*. A wedge-like sector, indicated by *blue arrows*, appears to be relatively spared from disease-related changes in P9 (**c**) and P10 (**d**).

Investigative Ophthalmology & Visual Science

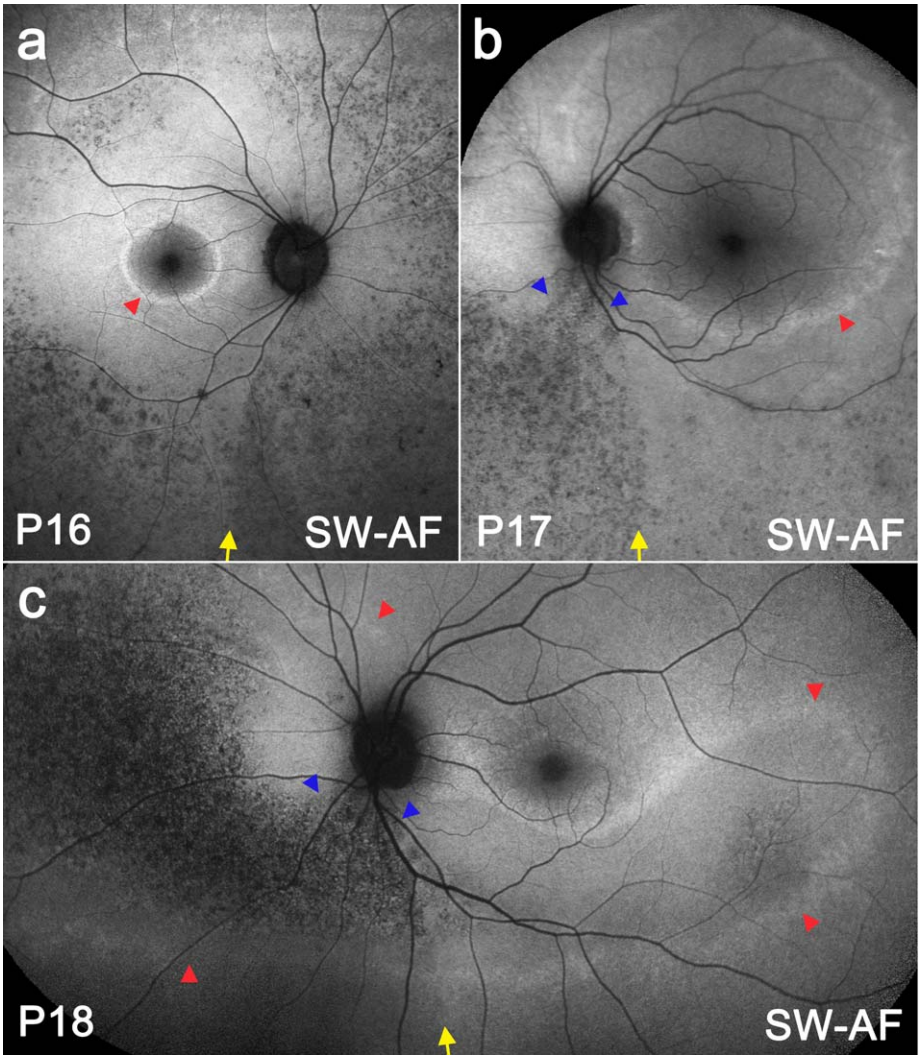

FIGURE 6. SW-AF images and fundus montages of RP patients P16 (**a**), P17 (**b**), and P18 (**c**). Each patient has a ring/band of increased SW-AF (*red arrowheads*). The optic fissure-related demarcation line is indicated by a *yellow arrow*. The inferonasal area of mottled low SW-AF changes is connected to the inferior part of the optic disc in P17 (**b**) and P18 (**c**) forming a wedge (*blue arrowheads*).

optic disc and terminate inferiorly at the demarcation line (yellow arrow). In P8 (Fig. 5b), a chain of flecks line up at the temporal edge of the demarcation line (yellow arrow). Patients P9 (Fig. 5c) and P10 (Fig. 5d) both demonstrate a wedge-shaped corridor (blue arrowheads) nasal to the demarcation line (yellow arrow) that is relatively spared of flecks and other disease-related changes.

In the nonnormalized SW-AF images of STGD1 patients (10 eyes), the nasal versus temporal GL ratio, 20° inferior to the optic disc was 0.75 ± 0.11 (mean ± SD), significantly lower (higher contrast) than the 0.87 ± 0.06 (mean ± SD) observed in healthy subjects[9] (Mann-Whitney U test, $P = 0.0009$). In corresponding non-normalized NIR-AF images (5 eyes), the nasal versus temporal GL ratio at the same locations was 0.82 ± 0.12 (mean ± SD). The ratios from the SW-AF and NIR-AF images were not significantly different from each other (Mann-Whitney U test, $P = 0.2544$).

Retinitis Pigmentosa

Figure 6 shows three RP patients. Patients P16 (Fig. 6a) and P17 (Fig. 6b) demonstrate a high SW-AF ring (red arrowheads), which encloses a central area of normal-appearing SW-AF. In P18 (Fig. 6c), a case of sector RP, a continuous high SW-AF band (red arrowheads) outlines the affected retina, which spans an arc from the nasal retina and around the optic disc to the retina inferior and temporal to the macula. In all cases, a speckled low SW-AF pattern can be observed inferior to the optic disc that is more pronounced than the pattern observed temporally. The patterned area forms a wedge (blue arrowheads) in P17 (Fig. 6b) and P18 (Fig. 6c). The temporal border of this low SW-AF area (yellow arrows) correlates with the position of the demarcation line observed in healthy subjects and STGD1 patients. Noticeably, the high SW-AF band present in P18 (red arrowheads) crossed the demarcation line without interruption (Fig. 6c).

DISCUSSION

The closed optic fissure, which has recently been shown to influence the spatial distribution of SW-AF in the inferonasal fundi of normal subjects,[9] also appears to serve as a boundary for some, but not all, abnormal AF patterns in STGD1 and RP. For instance, in RP, which is characterized by progressive photoreceptor degeneration, a high SW-AF band at the

transition zone between affected and unaffected retina, continued across the closed optic fissure without interruption in P18 (Fig. 6c). This band is thought to originate from dying photoreceptor cells.[19] Thus, the disease pattern generated at the photoreceptor cell level does not seem to be affected by the optic fissure. Conversely, low SW-AF patterns in RP that likely reflect RPE changes (e.g., pigmented cell migration) were markedly dissimilar on one side of the fissure versus the other. Similarly, in STGD1, AF flecks and areas of mottled AF patterns respect the demarcation line as a boundary.

All STGD1 patients we studied exhibited a demarcation line inferior to the optic disc; this boundary separated higher SW-AF levels on the temporal side from lower SW-AF levels nasally. Since the spatial distribution of SW-AF closely follows the distribution of rods,[20] actual differences in lipofuscin levels on the nasal versus the temporal side could occur if there were increased photoreceptor cell numbers temporally. To the best of our knowledge, however, there is no evidence to support this assumption. We have previously suggested that even if lipofuscin levels were not actually different on one side of the optic fissure versus the other, an apparent difference could manifest due to regional differences in size and shape of RPE cells.[9]

NIR-AF is considered to originate from melanin in RPE and choroidal melanocytes, with NIR-AF emission from the choroid being greater than the corresponding emission from the RPE in the healthy eye.[15] In areas of extensive RPE atrophy in STGD1, choroidal details become visible in NIR-AF images.[16] Conversely, when atrophy is absent in STGD1 patients, the intact RPE monolayer reduces the visibility of choroidal vessels (Figs. 3f–j) as compared with healthy subjects (Figs. 2f–j). In color fundus images, the fundus exhibits a brighter red on the nasal side of the fissure demarcation line, presumably because of a lower melanin content of RPE cells in this area.[9] Of interest, however, while this nasal-temporal difference in melanin does not reach detectability by NIR-AF imaging in healthy eyes,[9] in STGD1 patients, the NIR-AF signal is lower nasally than temporally, and consequently a demarcation line at the position of the closed optic fissure becomes visible.

In STGD1, the SW-AF emission at the fundus is increased due to augmented RPE lipofuscin.[7] But what is the basis for the increase in NIR-AF signal in STGD1[21] versus healthy eyes, and why does the inferonasal demarcation line become visible in NIR-AF images of STGD1 patients? While there is no evidence that RPE lipofuscin can absorb and emit fluorescence in the NIR range, we have previously suggested that the distribution of lipofuscin granules relative to melanosomes in the RPE cell may allow lipofuscin to modulate the NIR-AF signal originating from melanin.[22] In keeping with this notion, the lower nasal-temporal ratio (more contrast) in SW-AF intensity at the fissure in STGD1 patients (0.75 ± 0.11) versus healthy controls (0.87 ± 0.06)[9] could explain the visibility of the fissure in NIR-AF images. NIR-AF could be modulated by RPE lipofuscin or melanolipofuscin. While the mechanism by which the fissure becomes visible in NIR-AF images in STGD1 is not certain, this feature can potentially be used as a clinical diagnostic tool and help to identify STGD1 patients.

The findings in this study were made in a relatively small group of patients. It would be interesting to examine a significantly larger group of STGD1 patients to statistically assess the clinical utility of the visibility of the optic fissure by NIR-AF as a diagnostic tool. A future study could investigate, whether this fundus feature facilitates the differentiation between *ABCA4* and non-*ABCA4* related disease in otherwise similar phenotypes (e.g., in bull's-eye maculopathy and in cases where both pattern dystrophy and STGD1 are considered as diagnoses[23]). It is also important to note that only a small group of selected RP patients were included in this study. Thus, the finding that patterns of mottled SW-AF can respect the optic fissure as a boundary may only be evident in certain phenotypes.

Acknowledgments

The authors thank François C. Delori, Schepens Eye Research Institute and Department of Ophthalmology, Harvard Medical School, Boston, Massachusetts, for suggestions regarding the manuscript.

Supported by National Eye Institute/National Institutes of Health Grants EY019007 and EY019861, the Foundation Fighting Blindness, and an unrestricted grant from Research to Prevent Blindness to the Department of Ophthalmology, Columbia University.

Disclosure: **T. Duncker**, None; **W. Lee**, None; **S.H. Tsang**, None; **J.P. Greenberg**, None; **J. Zernant**, None; **R. Allikmets**, None; **J.R. Sparrow**, None

References

1. Delori FC, Dorey CK, Staurenghi G, Arend O, Goger DG, Weiter JJ. In vivo fluorescence of the ocular fundus exhibits retinal pigment epithelium lipofuscin characteristics. *Invest Ophthalmol Vis Sci*. 1995;36:718–729.
2. Eagle RC Jr, Lucier AC, Bernardino VB Jr, Yanoff M. Retinal pigment epithelial abnormalities in fundus flavimaculatus: a light and electron microscopic study. *Ophthalmology*. 1980; 87:1189–1200.
3. Allikmets R, Singh N, Sun H, et al. A photoreceptor cell-specific ATP-binding transporter gene (ABCR) is mutated in recessive Stargardt macular dystrophy. *Nat Genet*. 1997;15: 236–246.
4. Azarian SM, Travis GH. The photoreceptor rim protein is an ABC transporter encoded by the gene for recessive Stargardt's disease (ABCR). *FEBS Lett*. 1997;409:247–252.
5. Molday LL, Rabin AR, Molday RS. ABCR expression in foveal cone photoreceptors and its role in Stargardt macular dystrophy. *Nat Genet*. 2000;25:257–258.
6. Sun H, Nathans J. Stargardt's ABCR is localized to the disc membrane of retinal rod outer segments. *Nat Genet*. 1997;17: 15–16.
7. Delori FC, Staurenghi G, Arend O, Dorey CK, Goger DG, Weiter JJ. In vivo measurement of lipofuscin in Stargardt's disease—fundus flavimaculatus. *Invest Ophthalmol Vis Sci*. 1995;36:2327–2331.
8. Cukras CA, Wong WT, Caruso R, Cunningham D, Zein W, Sieving PA. Centrifugal expansion of fundus autofluorescence patterns in Stargardt disease over time. *Arch Ophthalmol*. 2012;130:171–179.
9. Duncker T, Greenberg JP, Sparrow JR, Smith RT, Quigley HA, Delori FC. Visualization of the optic fissure in short-wavelength autofluorescence images of the fundus. *Invest Ophthalmol Vis Sci*. 2012;53:6682–6686.
10. Heussen FM, Tan CS, Sadda SR. Prevalence of peripheral abnormalities on ultra-widefield greenlight (532 nm) autofluorescence imaging at a tertiary care center. *Invest Ophthalmol Vis Sci*. 2012;53:6526–6531.
11. Oishi A, Ogino K, Makiyama Y, Nakagawa S, Kurimoto M, Yoshimura N. Wide-field fundus autofluorescence imaging of retinitis pigmentosa. *Ophthalmology*. 2013;120:1827–1834.
12. Witmer MT, Kiss S. Wide-field imaging of the retina. *Surv Ophthalmol*. 2013;58:143–154
13. Delori F, Greenberg JP, Woods RL, et al. Quantitative measurements of autofluorescence with the scanning laser ophthalmoscope. *Invest Ophthalmol Vis Sci*. 2011;52:9379–9390.

14. Aleman TS, Cideciyan AV, Sumaroka A, et al. Retinal laminar architecture in human retinitis pigmentosa caused by rhodopsin gene mutations. *Invest Ophthalmol Vis Sci*. 2008;49:1580–1590.
15. Keilhauer CN, Delori FC. Near-infrared autofluorescence imaging of the fundus: visualization of ocular melanin. *Invest Ophthalmol Vis Sci*. 2006;47:3556–3564.
16. Kellner S, Kellner U, Weber BH, Fiebig B, Weinitz S, Ruether K. Lipofuscin- and melanin-related fundus autofluorescence in patients with ABCA4-associated retinal dystrophies. *Am J Ophthalmol*. 2009;147:895–902.902.e891.
17. Kellner U, Kellner S, Weber BH, Fiebig B, Weinitz S, Ruether K. Lipofuscin- and melanin-related fundus autofluorescence visualize different retinal pigment epithelial alterations in patients with retinitis pigmentosa. *Eye (Lond)*. 2009;23:1349–1359.
18. Weinberger AW, Lappas A, Kirschkamp T, et al. Fundus near infrared fluorescence correlates with fundus near infrared reflectance. *Invest Ophthalmol Vis Sci*. 2006;47:3098–3108.
19. Sparrow JR, Yoon KD, Wu Y, Yamamoto K. Interpretations of fundus autofluorescence from studies of the bisretinoids of the retina. *Invest Ophthalmol Vis Sci*. 2010;51:4351–4357.
20. Delori FC, Goger DG, Dorey CK. Age-related accumulation and spatial distribution of lipofuscin in RPE of normal subjects. *Invest Ophthalmol Vis Sci*. 2001;42:1855–1866.
21. Cideciyan AV, Swider M, Aleman TS, et al. Reduced-illuminance autofluorescence imaging in ABCA4-associated retinal degenerations. *J Opt Soc Am A Opt Image Sci Vis*. 2007;24:1457–1467.
22. Duncker T, Tabacaru MR, Lee W, Tsang SH, Sparrow JR, Greenstein VC. Comparison of near-infrared and short-wavelength autofluorescence in retinitis pigmentosa. *Invest Ophthalmol Vis Sci*. 2013;54:585–591.
23. Boon CJ, van Schooneveld MJ, den Hollander AI, et al. Mutations in the peripherin/RDS gene are an important cause of multifocal pattern dystrophy simulating STGD1/fundus flavimaculatus. *Br J Ophthalmol*. 2007;91:1504–1511.

Investigative Ophthalmology & Visual Science